Journal of Structural Geology 32 (2010) 28–44

Contents lists available at ScienceDirect

Journal of Structural Geology

journal homepage: www.elsevier.com/locate/jsg

Load and unload as interference factors on cyclical behavior and kinematics of Coulomb wedges: Insights from sandbox experiments

S. Bigi [a,*], L. Di Paolo [b], L. Vadacca [a], G. Gambardella [a]

[a] Dipartimento Scienze della Terra, Sapienza Università di Roma, P.le A. Moro, 5 – 00183, Roma, Italy
[b] Dipartimento di Geologia, Università di Roma Tre, L.go S. Murialdo, 5 – 00147 Roma, Italy

ARTICLE INFO

Article history:
Received 1 September 2008
Received in revised form
13 May 2009
Accepted 29 June 2009
Available online 9 July 2009

Keywords:
Analogue model
Critical taper
Accretion mode
Sedimentation
Erosion

ABSTRACT

Modes of accretion in orogenic wedges are strongly controlled by mass balance and the efficiency of basal detachment. Sandbox models of accretionary wedges have demonstrated that fault systems grow episodically via cycles of alternating wedge thickening and lengthening. Generally, a new thrust plane generates within the footwall of the previous one, following a piggy-back mode of accretion, whereas redistribution of the mass balance in the wedge is associated to underthrusting and the reactivation of previous thrusts.

We present the results of five sandbox experiments that model the interaction between tectonic accretion, sedimentation in foredeep area and erosion in the axial zone, in order to analyze the influence of these events on the cyclical behavior of a growing wedge. Modifications of the initial setup were made to analyze the effect on wedge development of syntectonic denudation, syntectonic sedimentation and coeval sedimentation and erosion, which markedly altered mass transfer within the wedge. In particular, lowering the surface slope by syntectonic erosion triggered synchronous accretion and underthrusting modes; by contrast, a sudden syntectonic sediment load in the prowedge region promoted prolonged phases of underthrusting, retarding the accretion of new imbricates at the prowedge toe, whether wedge volume was increased or not.

The high length/thickness ratio of the model (120 cm/2.5 cm) allowed us to monitor a complete cycle of recovery of the system after each episode of sedimentation and/or erosion, observing how the wedge reacted to modification both altering its own cyclicity and progressively recovering it.

1. Introduction

Thin-skinned thrust belts and accretionary wedges form at convergent plate margins by horizontal shortening and vertical thickening of sedimentary strata. In response to horizontal compression, sedimentary sequences undergo thrust faulting, which is the main mechanism of deformation. At the same time, especially in continental convergence settings, both the lithospheric flexure and the superficial processes, as syntectonic sedimentation and erosion, control the kinematic behavior of orogenic wedges. Critical taper theory has proven very effecting in linking the force balance of a growing orogenic wedge and its bulk geometry, mechanical properties, and kinematics (Chapple, 1978; Davis et al., 1983; Dahlen, 1984; Dahlen et al., 1984). This approach has been successfully used to explain the mechanics of fold-and-thrust belts, forearc wedges and entire orogenic belts (Davis et al., 1983; Dahlen et al., 1984; Dahlen, 1990; Platt, 1988; Willet, 1992). Scaled analogue experiments with granular materials (e.g. sand) link the internal structural evolution of the wedge to the material properties, thereby yielding a first-order approach to understanding the mechanics of different deformation styles present in nature (Malavieille, 1984; Liu et al., 1992; Lallemand et al., 1994; Koyi, 1995; Gutscher et al., 1996, 1998; Wang and Davis, 1996).

Accretionary wedges or fold-and-thrust belts, as well as sand wedges, are described in terms of the critical angle (θ), defined as the sum of the dip of the wedge topography (α) and the dip of basal detachment (β). The theory of critical taper predicts that the coefficients of friction of both the wedge material (μ) and basal detachment (μ_b) control the variation of these angles. Simple variations in the μ/μ_b ratio, in fact, allow the derived equations to describe the complete sequence of faulting processes occurring at contractional margins. Moreover, according to the theory, processes of deformation progressively vary the shape of the wedge until it reaches the critical taper value (Davis et al., 1983; Dahlen, 1984; Dahlen et al., 1984). Despite this theoretical prediction, the observed variation of critical taper values in analogue models and in natural

* Corresponding author. Tel.: +39 06 49914922; fax: +39 06 4454729.
E-mail address: sabina.bigi@uniroma1.it (S. Bigi).

0191-8141/$ – see front matter © 2009 Elsevier Ltd. All rights reserved.
doi:10.1016/j.jsg.2009.06.018

wedges shows a cyclical behavior, characterized by discontinuous phases of alternating wedge thickening, accommodated by slip along thrust faults within the wedge, and wedge lengthening, accommodated by nucleation of new thrust faults in front of the wedge (Mulugeta and Koyi, 1992; Storti and McClay, 1995; Gutscher et al., 1996; McClay and Whitehouse, 2004; Konstantinovskaia and Malavieille, 2005; Del Castello and Cooke, 2007). These two processes, referred to as underthrusting and accretion, progressively reduce the θ variation, until it reaches a constant critical value (Mulugeta and Koyi, 1992), and, in those analogue models where the dip angle of the basal detachment is assumed to be constant ($\beta = 0$), the dip of the topographic slope α becomes the only observed critical parameter. This makes it possible to observe the way in which the (α) value and the wedge itself react to potential interference factors affecting the system. Ramp spacing and the length of the wedge are other parameters that show a cyclical behavior during deformation; for these, too, a general re-organization can be observed after a modification of the system.

Syntectonic sedimentation and erosion strongly influence the mechanical balance of foreland thrust-and-fold belts and accretionary prisms and, consequently, their α value and wedge kinematics (Davis et al., 1983; Willet et al., 1993; Beaumont et al., 1999; Storti et al., 2000; Graveleau and Dominguez, 2008). Using sandbox modeling, several authors have focused their analysis on the erosion located at the top of double-verging wedges (Muñoz, 1992; McClay et al., 1999; McClay and Whitehouse, 2004), on syntectonic sedimentation (Storti et al., 1995; Mugnier et al., 1997), and on the interaction between tectonics, erosion and sedimentation in the forearc region of accretionary wedges or in a foreland thrust belts (Malavieille et al., 1993; Larroque et al., 1995; Graveleau and Dominguez, 2008).

We have used experimental models to study synchronous sedimentation and/or erosion and shortening of sand wedges, analyzing the interaction between fold-and-thrust belt construction and foredeep basin development. The experimental apparatus has a general configuration similar to the one used to simulate a double-verging wedge characterized by reversal kinematics occurring in two stages (Liu et al., 1992; Storti et al., 1995, 2000; Persson and Sokoutis, 2002).

We focused our analysis mostly on the second stage of wedge evolution, characterized by the propagation of thrusting in the prowedge (*sensu* Storti et al., 2000). The length of the experimental apparatus allows us to simulate an asymmetric wedge, where the prowedge area is more developed than the retrowedge. This configuration is more effective for the analysis of the cyclical behavior of the critical parameters in question because it allows the observation of the whole recovery process of the wedge after every episode of erosion and/or sedimentation.

We considered the axial and the retrowedge zones as the equivalents of the inner zones of a chain, where contractional deformation acts mainly before the prowedge development and where the subsequent deformation acts as the result of the general mass and force balance. The resulting strongly asymmetric wedges are remindful of natural examples such as the Apennines and the Carpathians in continental settings (Doglioni et al., 1999) or the Banda Arc and the Barbados in oceanic settings (Westbrook et al., 1988; Bigi et al., 2003; Lenci and Doglioni, 2007), characterized by well-developed fold-and-thrust belts with respect to a double-verging inner part of the chain. The origin of the double-verging inner part of natural wedges is largely debated and interpreted in different ways; the west-dipping subduction of continental and or oceanic crust, the continental collision, the inversion of intraplate extensional basin, as well as the switch of subduction polarity are among the most common proposed models (e.g. Doglioni et al., 1999; Frizon De Lamotte, 2005; Muñoz, 1992). Whether or not the double-verging inner area is genetically connected to the subduction (as was the case in our models), the initial configuration adopted allows one to verify if, when and how the retrowedge area undergoes deformation connected to the evolution of the fold-and-thrust belt in the prowedge (i.e. uplift, erosion, out-of-sequence thrusting, extension).

The localization of sedimentation in the external part of the developing prowedge simulates the role of sedimentation in a foredeep domain, although our experiments cannot account for isostatic subsidence and its mechanical effects. Foredeep basins can be considered critical features in the evolution of fold-and-thrust-belts because they are sites of repeated events of syntectonic loading on the sole thrust of the orogen and on the still undeformed foreland (De Celles and Giles, 1996). We performed the first experiment E1 using a base configuration, repeated in all other experiments, without altering the system in order to use it as a reference frame. We simulated a single episode of sedimentary loading in experiment E2, and repeated episodes of loading in experiment E3; in experiments E4, the role of erosion at the top of the wedge in the inner part of a chain was simulated. As most fold-and-thrust belts show erosion in the axial area and sedimentation in the foredeep domain, we also combined these two processes in experiment E5, in order to simulate the mass transfer occurring from the inner part to the external part of the wedge during deformation.

2. Experimental method and model parameters

The apparatus used for these experiments was a deformation rig 2.40 m long; on the sides are two adjustable glass panes which allow one to choose the width of the rig, whereas the two ends of the rig are open (Fig. 1). All experiments were performed in normal gravity conditions. Dry, non-cohesive quartz sand with 190 μm grain size (coefficient of friction $\mu = 0.55$) (McClay, 1990; Liu et al., 1992) and an average density of 1.58 ± 0.1 g cm^{-3} in the conditions of deposition within the experimental apparatus, was used to simulate the brittle deformation of sedimentary rocks in accretionary prisms or thrust wedges (Storti, 1997). The drafting film used to simulate the basal detachment was characterized by a high coefficient of friction ($\mu_b = 0.55$) equal to the coefficient of friction of quartz sand (McClay et al., 1999). Based on a scaling factor of 10^{-5}, 1 cm in the models represents ~1 km in upper-crustal rocks (Liu et al., 1992). In all experiments, an initial sand pack 160 cm × 43.8 cm × 2.5 cm was constructed manually, trying to minimize local inhomogeneities and packing anisotropy, and alternating black and white layers of sand. Green and red sand simulated the syn-contractional strata. The glass panes were cleaned and coated with a transparent, friction-reducing synthetic compound to minimize sidewall friction to negligible quantities and making it possible to obtain an optimal recording of deformation increments. At the end of each experiment, the deformed sand pack was consolidated with water, cut into 5 cm wide slides, and photographed, in order to verify the correspondence of internal geometries with those observed through the lateral glass panes.

The experiment configuration is the same used to simulate double-verging wedges (Storti et al., 2000), where deformation is induced within the sand pack by pulling with a motor drive the basal decollement sheet (6.67 cm h^{-1}) down into a thin subduction slot (S) located 120 cm from the front end of the sand layer apparatus (Fig. 1). The bottom of the deformation rig, from the subduction slot (S) to the back end of the apparatus (40 cm) was floored with the same drafting film in order to ensure the same basal frictional characteristics throughout the entire model. Cumulative displacement for each thrust fault was plotted against a shortening ratio, expressed in terms of $S_h = L_1/L_0 \times 100$, where L_0 is the initial sand pack length and L_1 is the progressive shortening applied to the sand

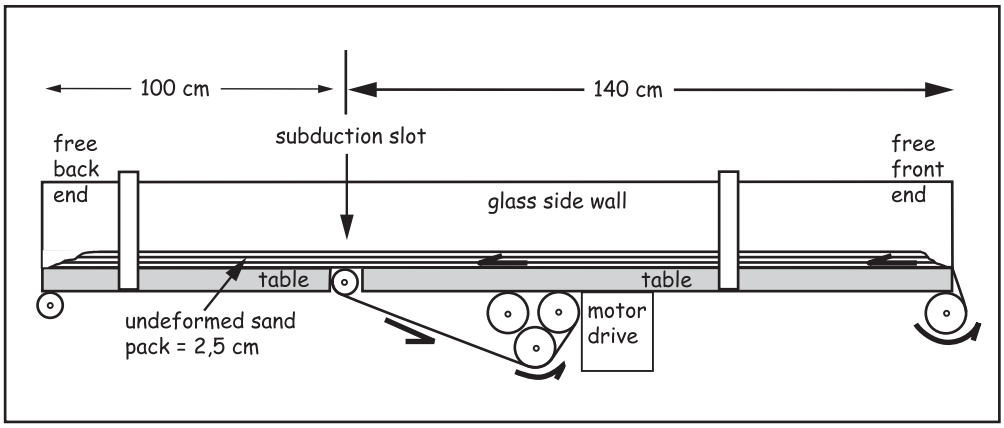

Fig. 1. Diagram of the experimental apparatus. The total length of the rig is 2.40 cm, and the thickness of the sand pack is 2.5 cm. The two glass side walls were positioned at a distance of 43.8 cm each other for all the experiments.

pack. Deformation was recorded by time-lapse photography at every 1% of deformation increment, corresponding to 1.4 cm. The experiments ended when a stable wedge formed and slid on the basal detachment with no further internal deformation (Liu et al., 1992).

In all the experiments, the adoption of a high length/thickness ratio (140 cm/2.5 cm) allowed us to observe how the wedge recovers stability after each episode of sedimentation/erosion.

The measured parameters were (Fig. 2): displacement along each thrust ramp (T_n) using the displacement of the intermediate horizon, height reached by the axial zone (H), length of prowedge and retrowedge (L_p and L_r, respectively).

According to Storti et al. (2000), we define the prowedge as the region in front of the subduction slot (S), where material moves toward S and the dominant tectonic transport direction is opposite to the motion of the detachment sheet. The retrowedge is the region behind the subduction slot, where there is no relative motion between the rigid basal plate and the undeformed material and where the drifting film is fixed. The flat region, between the prowedge and the retrowedge, is the axial zone. The subscript n indicates the order of nucleation of the thrust ramps in the prowedge. H_0 is the height of the undeformed multilayer.

Three α values have been measured to describe the topographic surface in different sectors of the wedge: i) retrowedge (α_r), axial zone (α) and prowedge (α_p). These three domains show different kinematics during deformation (Storti et al., 2000; Del Castello et al., 2004). According to these authors, the zone of the retrowedge is made up mainly of slumped material from the axial zone and its slope (α_r) corresponds to the angle of repose of the sand multilayer. In the axial zone, the backward rotation of inactive thrusts causes vertical uplift rather than horizontal shortening, keeping the α value more or less constant. In the prowedge, where the active thrusts are, α_p shows a cyclical variation, eventually reaching critical surface, slope as new material is incorporated into the wedge and its volume increases (Fig. 2).

3. Experimental results

3.1. Model E1 – basic setup

Double-verging accretionary wedge as in model E1 show two stages of evolution as evidenced by the well documented models in literature (Malavieille, 1984; Mulugeta and Koyi, 1987; Mulugeta, 1988a,b; Liu et al., 1992; Calassou et al., 1993; Kukowski et al., 1994; Wang and Davis, 1996; Storti et al., 2000). The first part of the experiment E1, up to 10% of shortening, was in fact characterized by rapid uplift of the axial zone and by rapid thrusting along a retroverging thrust ramp, accompanied by the development of seven closely spaced pro-verging fault-related anticlines at the subduction slot, on which small percentages of shortening were partitioned (Fig. 3). The axial zone was located almost entirely within the region of the retrowedge because of the continuous deformation along the retroverging thrust ramp. The width of the flat-topped axial zone progressively decreased due to folding and slumping of material in the retrowedge. The deformation fronts of both the retrowedge and prowedge systems migrated outward at about at the same rate.

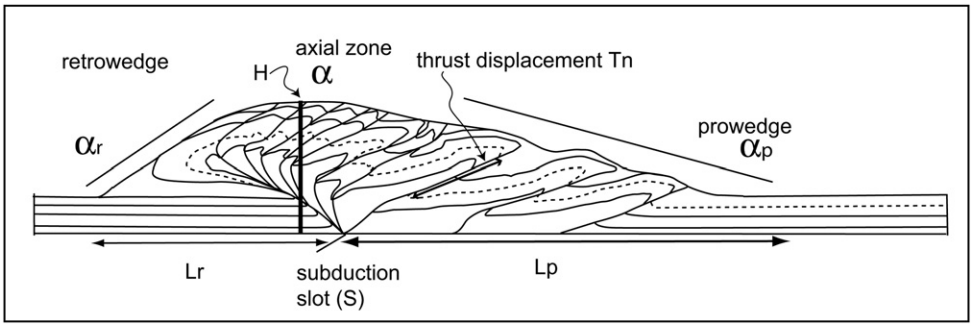

Fig. 2. Reference framework and parameters measured in the experimental wedge. The dip of the slope of the prowedge, of the retrowedge and of the axial zone is indicated with the greek letter α and the subscript, respectively, p, r and a. The distance between the active front and the subduction slot, measured along the basal detachment is indicated with the letter L, and the subscript p and r for respectively the prowedge and the retrowedge. The height H of the wedge and the displacement measured along the thrust plane are also indicated.

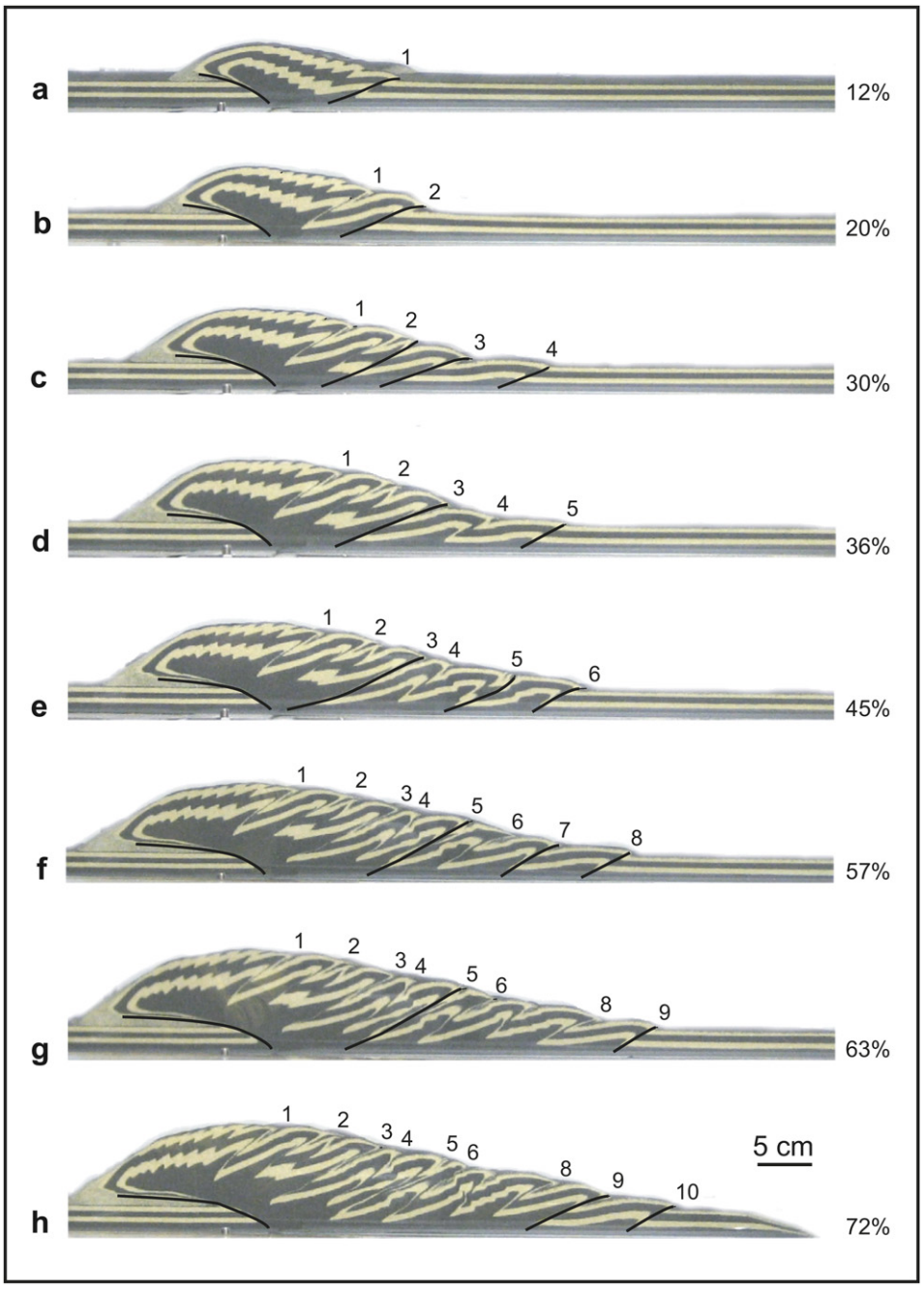

Fig. 3. Line drawing of the sequential evolution of the second stage of E1 model: a) 12% of shortening; b) 20%; c) 30%; d) 36%; e) 45%; f) 57%; g) 63%; h) 72%. The percentage of shortening is expressed in terms of $S_h = L_1/L_0 \times 100$, where L_0 is the initial sand pack length and L_1 is the progressive shortening applied to the sand pack. Thicker lines highlight active thrust at each stage of shortening.

After 10% of shortening, the evolution of the experiment changed abruptly: the eighth anticline nucleated in the prowedge far from the subduction slot and the deformation front stepped outward, while the retroverging thrusting temporarily stopped (Fig. 3). During this second stage, the evolutionary sequence consisted of the generation of ten, widely spaced, fault-related box folds at the toe of the prowedge far from the subduction slot (S), similar to thrust units (Mulugeta and Koyi, 1987). Uplift rate in the axial zone progressively decreased, due to faster and synchronous thrusting in the prowedge and slower thrusting in the retrowedge. The surface topography was strongly asymmetric with the increasing length of the prowedge (L_p) (Figs. 3 and 4).

The experiments ended at 72% of shortening (equals 100.8 cm), when the prowedge reached a critical angle of 10° (Figs. 3 and 4).

3.2. Model E2 – syntectonic sedimentation

In this experiment, we added syntectonic sedimentary strata at 40% of shortening, dropping coloured sand both on the growing prowedge and on the undeformed foreland, and decreasing the α value from 11° to 7° (Figs. 5 and 6).

At that moment, the model was already entered in the second evolution stage, and five fault-related folds had formed within the

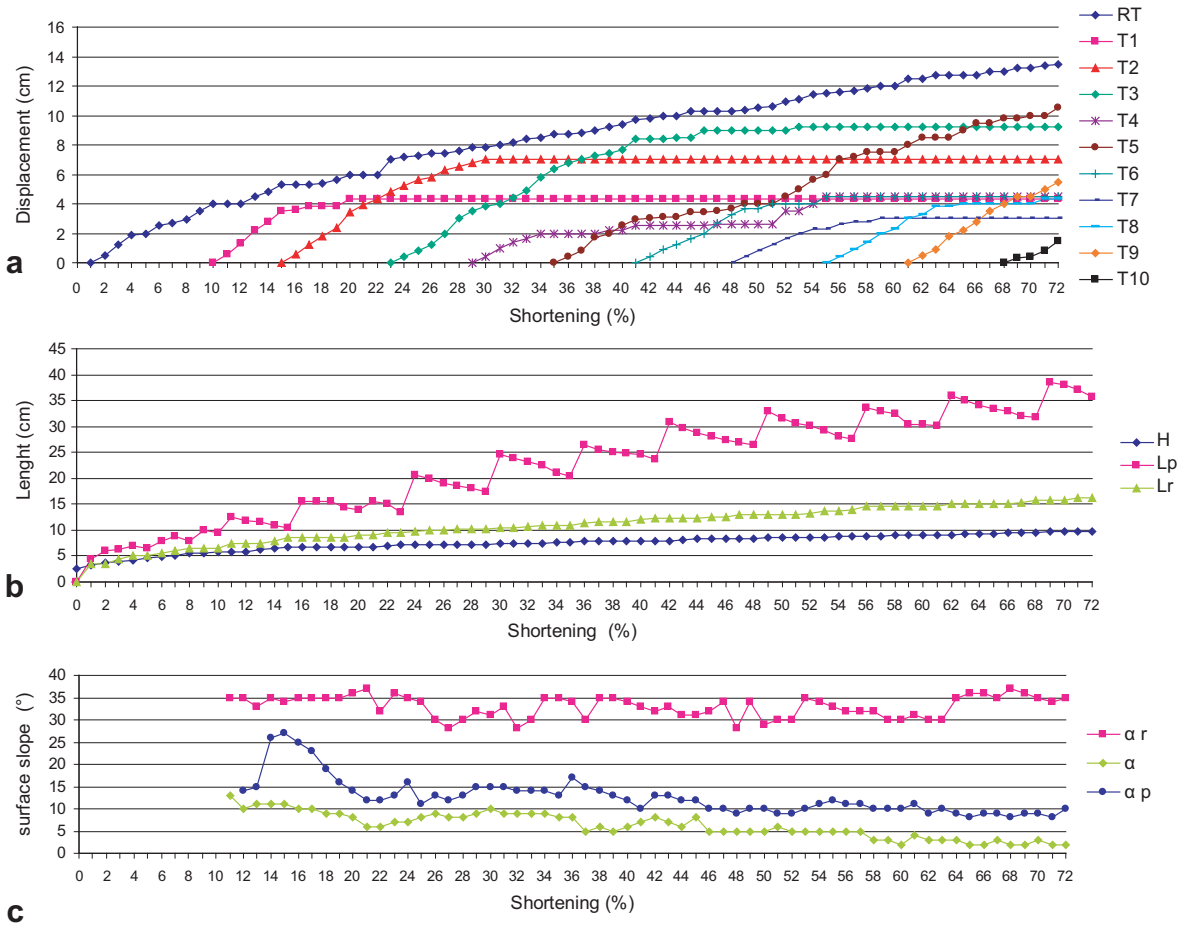

Fig. 4. Model E1. Progressive evolution of selected parameters vs. shortening: a) displacement along the retroverging ramp (RT) and along the main thrusts in the prowedge (T_n); b) height of the axial zone (H), distance of the deformation front in the prowedge (L_p) and in the retrowedge (L_r) from the subduction slot; c) surface taper of the prowedge (α_p), of the retrowedge (α_r) and of the axial zone (α).

prowedge, with a deformation rate comparable with the E1 experiment.

The added material was scaled in order to simulate a syntectonic wedge tapering above a basal surface inclined at 3° in the foreland and 5° on the wedge. Syntectonic sedimentation thickened the wedge in the area corresponding to the foreland basin including the wedge top and the axial area (*sensu* De Celles and Giles, 1996) and increased the load on the potential basal detachment, changing its basal frictional strength (Storti, 1997). The added material also modified the balance of strengths governing the dimension of newly created thrust sheets (Platt, 1988; Goff and Wiltschko, 1992).

After sedimentation, the displacement vs. shortening curves showed a reactivation of the preexistent thrusts and there was a long quiescent phase before the nucleation of a new thrust in the prowedge (Fig. 6). A marked re-activation of retrothrust (RT) immediately after the sedimentation event was observed, together with a fast advancing of the retrowedge toe (L_r), which, after 48% of deformation, reached 15 cm of length, which is the same length of the prowedge (L_p) (Fig. 6).

From 40% to 51% of shortening, the already formed thrusts (T4 and T5) remained active. At 49%, the deformation front stepped outward and the sixth anticline (T6) nucleated far from the subduction slot with a very long basal flat, restoring the former asymmetric shape of the wedge. Synchronously to the development of this main anticline, small thrusts nucleated using as detachment level the bottom of syntectonic sediments on the back limb of the growing anticlines. These more superficial thrusts cut through syn-contractional sediments at 42%, during T5 activity, and 53%, during T7 activity (Fig. 7). The experiment ended at 67% (93.8 cm) of shortening, when the wedge reached its critical angle equal to 9°, lower than the one in model E1 (Figs. 5 and 6).

3.3. Model E3 – repeated syntectonic sedimentation

We simulated syntectonic sedimentation in three different moments during the evolution of the wedge in order to model a repeated fill of a foreland basin (located on the prowedge and on the undeformed foreland). In a first-order of approximation, this procedure intends to represent natural conditions where the site of sedimentation is positioned close to the advancing wedge toe and corresponds to the point of maximum normal load on potential detachment (Del Castello et al., 2004). The first sedimentation event was simulated at 30% of shortening, the second at 43% and the third at 60% (Figs. 8 and 9), all of them after the beginning of the second stage of evolution. After the first sedimentary event, there was an immediate step back of the active deformation front, as already observed in experiment E2; the last thrust T5 ceased its activity between 30% and 32% of shortening, while a marked displacement on thrust T4 and on the retrothrust occurred (Fig. 9).

After this interval, T5 was reactivated and T4 stopped.

At 37% of shortening, a new ramp formed and, subsequently, the deformation localized on this new frontal anticline T6. As

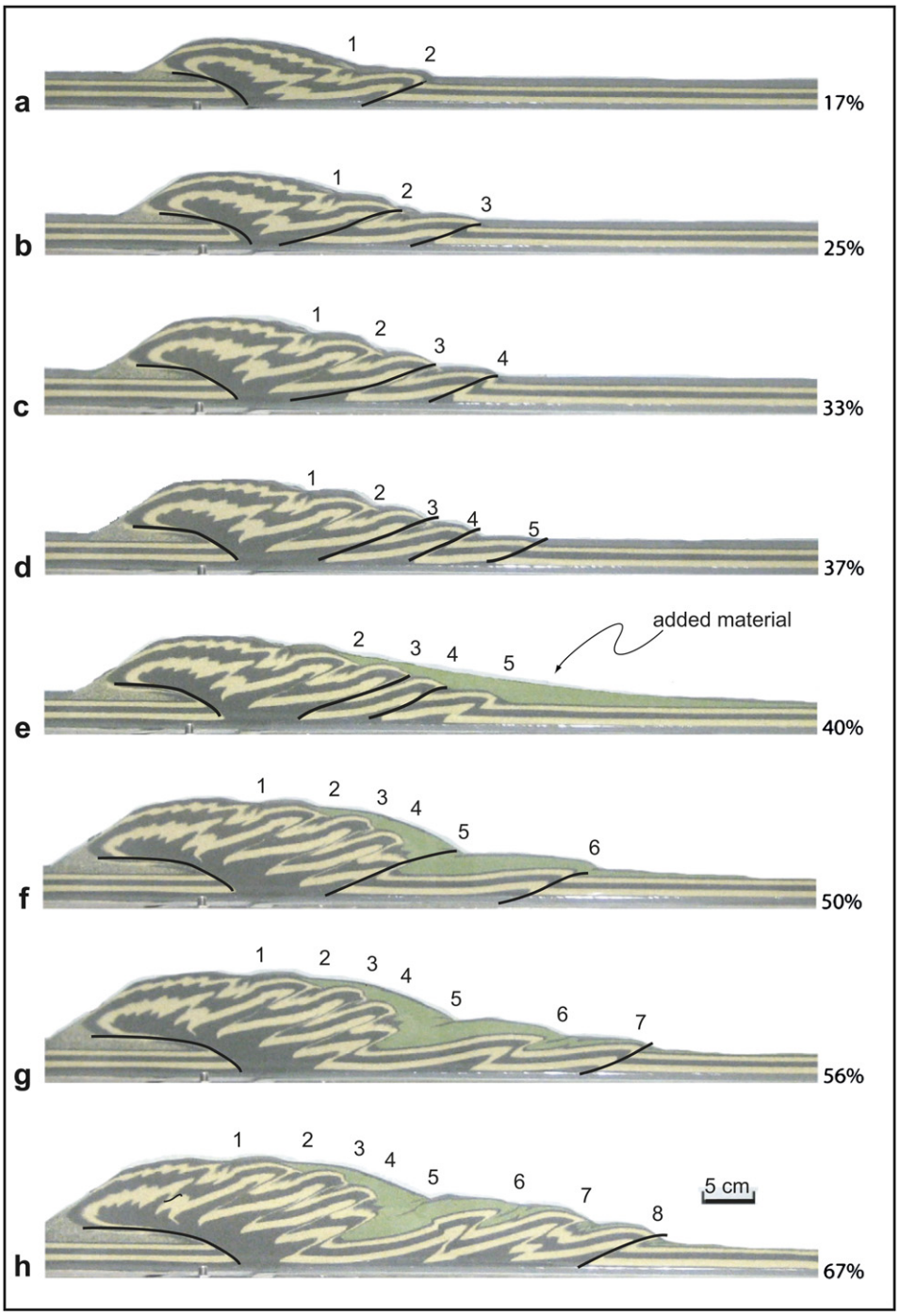

Fig. 5. Line drawing of the sequential evolution of second stage of E2 model: a) 17% of shortening; b) 25%; c) 33%; d) 37%; e) 40%; f) 50%; g) 56%; h) 67%. The added material is in light gray (green in the coloured version). Thicker lines highlight active thrust at each stage of shortening.

a consequence, part of the syntectonic sediments progressively deformed, setting the location of a piggy-back basin area (Fig. 8). Inside the syntectonic sediments a green reference bed had been layered to check these sediments were affected by the deformation; with increasing contraction, this marker level folded and formed a small syncline in the footwall of thrust fault T5.

At 43% of shortening, the second sedimentation event was imposed ahead of thrust T5, while a new ramp was going about to nucleate at a distance of approximately 11 cm from T6. This second sedimentary event re-activated thrust T5 and caused remarkable displacements on the retrothrust (Fig. 9).

At 50% of shortening, a new ramp (T7) formed far from the subduction slot, 11 cm ahead of the pre-existing protothrust, now buried under a thick syntectonic wedge. This new thrust nucleated on the basal detachment at the point of least shear resistance, at a distance of 22 cm from the previous thrust, followed by the nucleation of the last T8 thrust at 56% of shortening (Fig. 9). At 60% of shortening, the last sedimentary event was simulated. The added

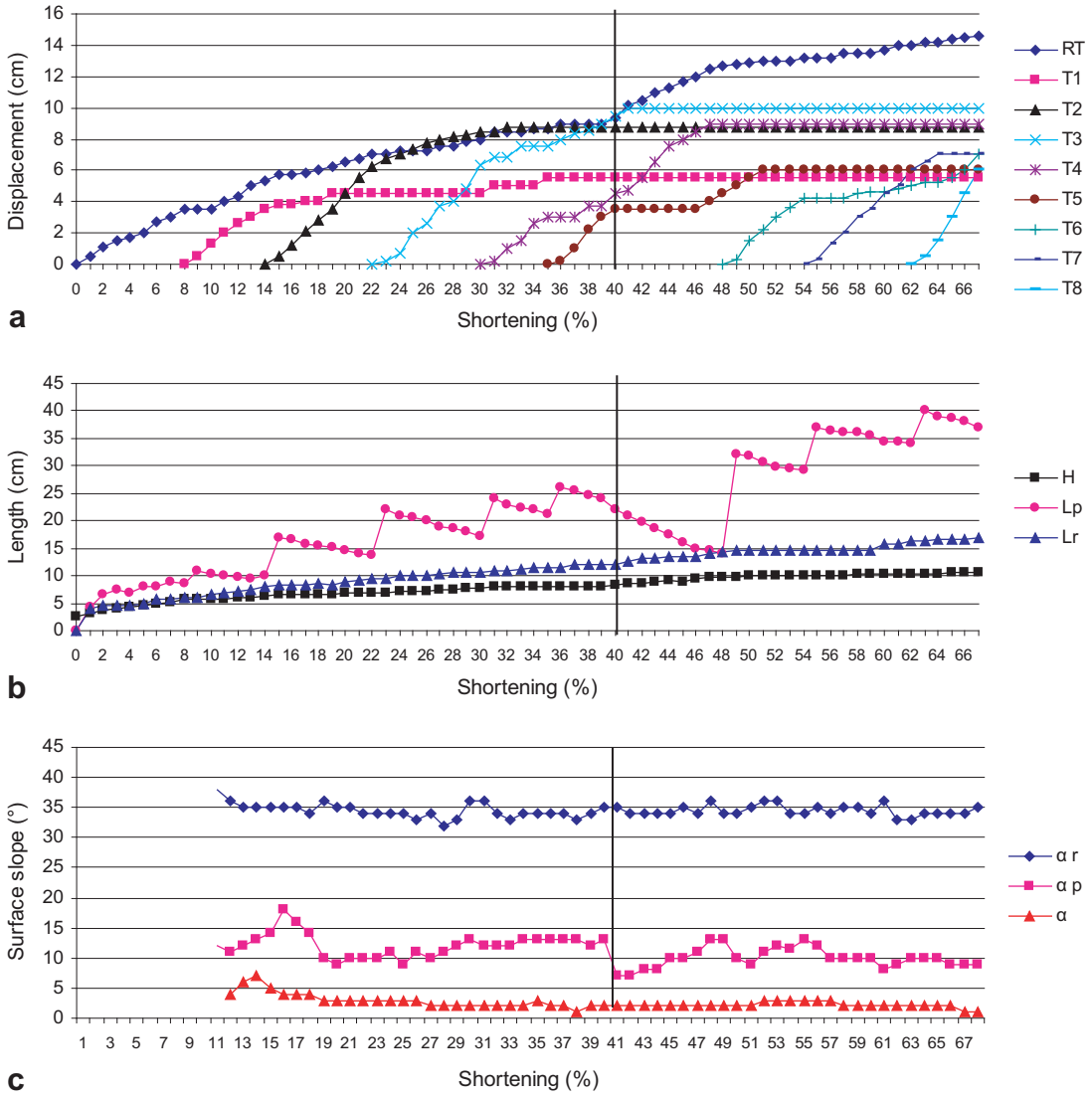

Fig. 6. Model E2. Progressive evolution of selected parameters vs. shortening: a) displacement along the retroverging ramp (RT) and along the main thrusts in the prowedge (T_n); b) height of the axial zone (H), distance of the deformation front in the prowedge (L_p) and in the retrowedge (L_r) from the subduction slot; c) surface taper of the prowedge (α_p), of the retrowedge (α_r) and of the axial zone (α). The syntectonic event, indicated as a vertical line on the diagrams, substantially delays the formation of sixth thrust T6, prolongs the quiescent phase of last thrust (T6), and strongly reactivates the fourth thrust T4 until to the nucleation of the sixth thrust at 48%. The steepening of the curve of RT, after the same event indicates the change of activity of the retrothrust.

material of this last sedimentation event was distributed from the axial zone to the end of the wedge in order to rectify the topographic profile of the prowedge, decreasing the slope value. This event of loading blocked off the activity of thrust T8 and re-activated thrusts T6, T7 and the retrothrust.

The experiment ended at 65% (91 cm) of shortening, when the wedge reached the critical state with a prowedge topographic slope equal to 8°, less than that reached in the first experiment (E1) (Fig. 8).

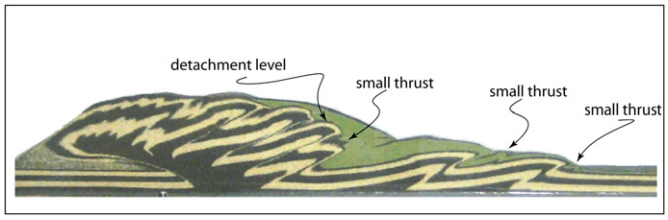

Fig. 7. Detail of experiment E2 at 58% of shortening. The small thrusts that nucleated from the bottom of the green added material are highlighted.

3.4. Model E4 – syntectonic erosion

Syntectonic erosion was modeled in experiment E4 at 40% of shortening, removing with a vacuum cleaner part of the pre-deformation sequence at the top of the wedge. The resulting erosional surface was horizontal, located at 6.1 cm from the bottom of the model, and is located on the axial zone, where, at this stage, only inactive thrusts were found (Fig. 10). Up to 40% of deformation, the evolution of the wedge was similar to former experiments (E1 and E2), being characterized by a two-stage evolution and the nucleation of five main thrust, forming respectively at 8%, 10%, 18%, 26% and 34% of shortening (Fig. 10). After 40% of shortening, the syntectonic erosion lowered the height value (H) from 8.1 cm to 6.1 cm, reducing the vertical load in the axial area and, therefore, basal frictional strength. Most of the wedge showed the same vertical thickness (about 6 cm), which modified the balance of strengths governing the

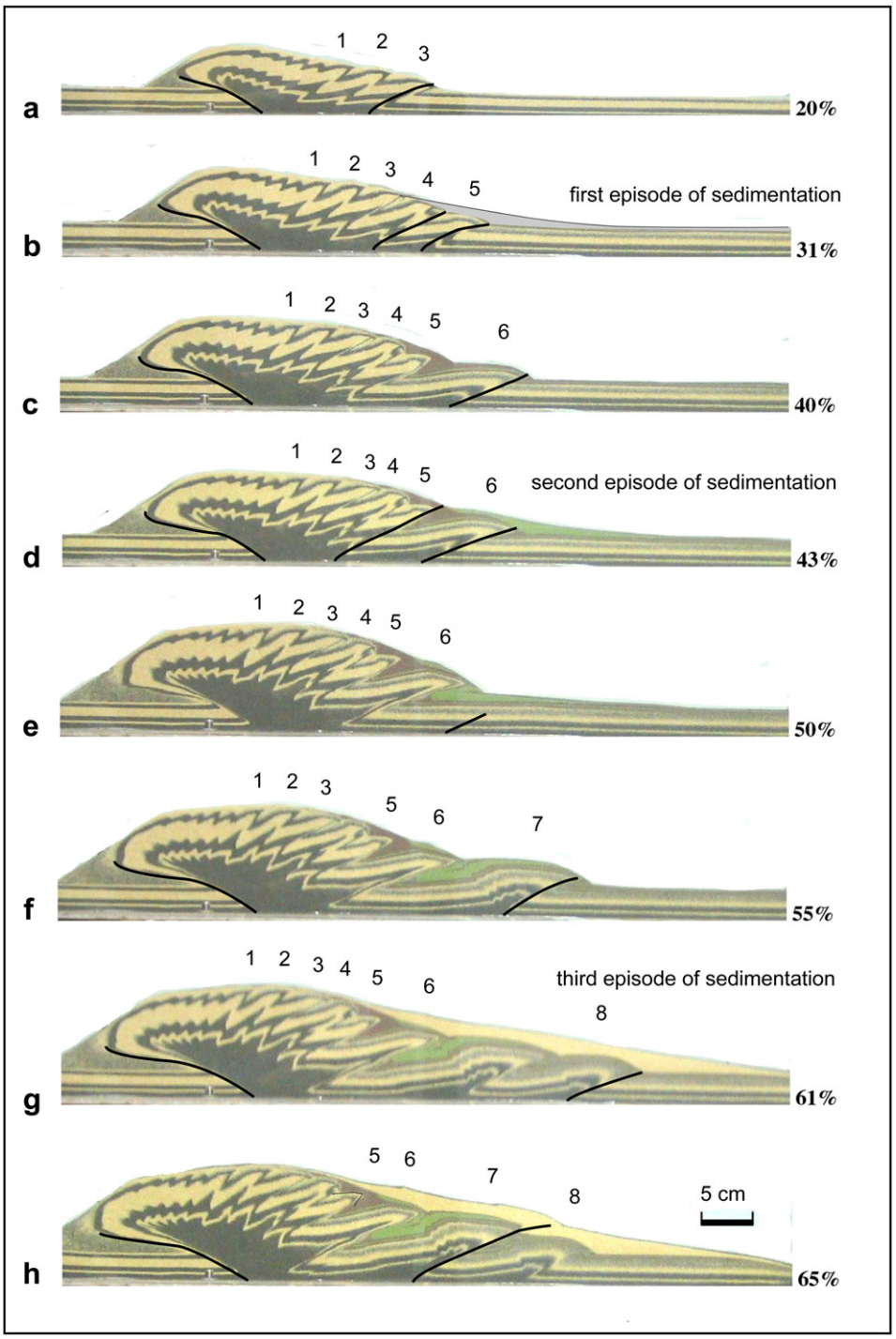

Fig. 8. Line drawing of the sequential evolution of the second stages of E3 model: a) 20% of shortening; b) 31%; c) 40%; d) 43%; e) 50%; f) 55%; g) 61%; h) 65%. The added material belonging to the three events of sedimentation (31%, 43% and 61%) are indicated with different gradation of gray (red, green and yellow in the coloured version). Thicker lines highlight active thrust at each stage of shortening.

kinematics of the wedge by imposing a rather uniform vertical load along the model (Fig. 10). The resulting geometry after imposed erosion was characterized by a very large and horizontal axial zone, the retrowedge slope showed a very steep angle ($\alpha_r = 35^\circ$) and so did the prowedge ($\alpha_p = 20^\circ$), which was located far from the subduction slot (S), at a distance of about 30 cm (Figs. 10 and 11).

After the erosional event both re-activation of preexisting thrusts, particularly T4 and T5, and propagation of the wedge occurred. At 42% of shortening the sixth thrust (T6), and at 49% the seventh thrust (T7), formed (Fig. 11). Differently from model E1, these thrusts remained active until the end of the experiment, cumulating great displacement. As already described, the erosive event produced several main effects: it increased the dip of topographic slope from 14° to 20°, it reduced the thickness of the internal part of the deforming wedge and redistributed the vertical load on the basal detachment. The observed reaction of the wedge was to reach again critical taper value and critical height, both by internal thrust reactivation and by new thrusting. Consequently,

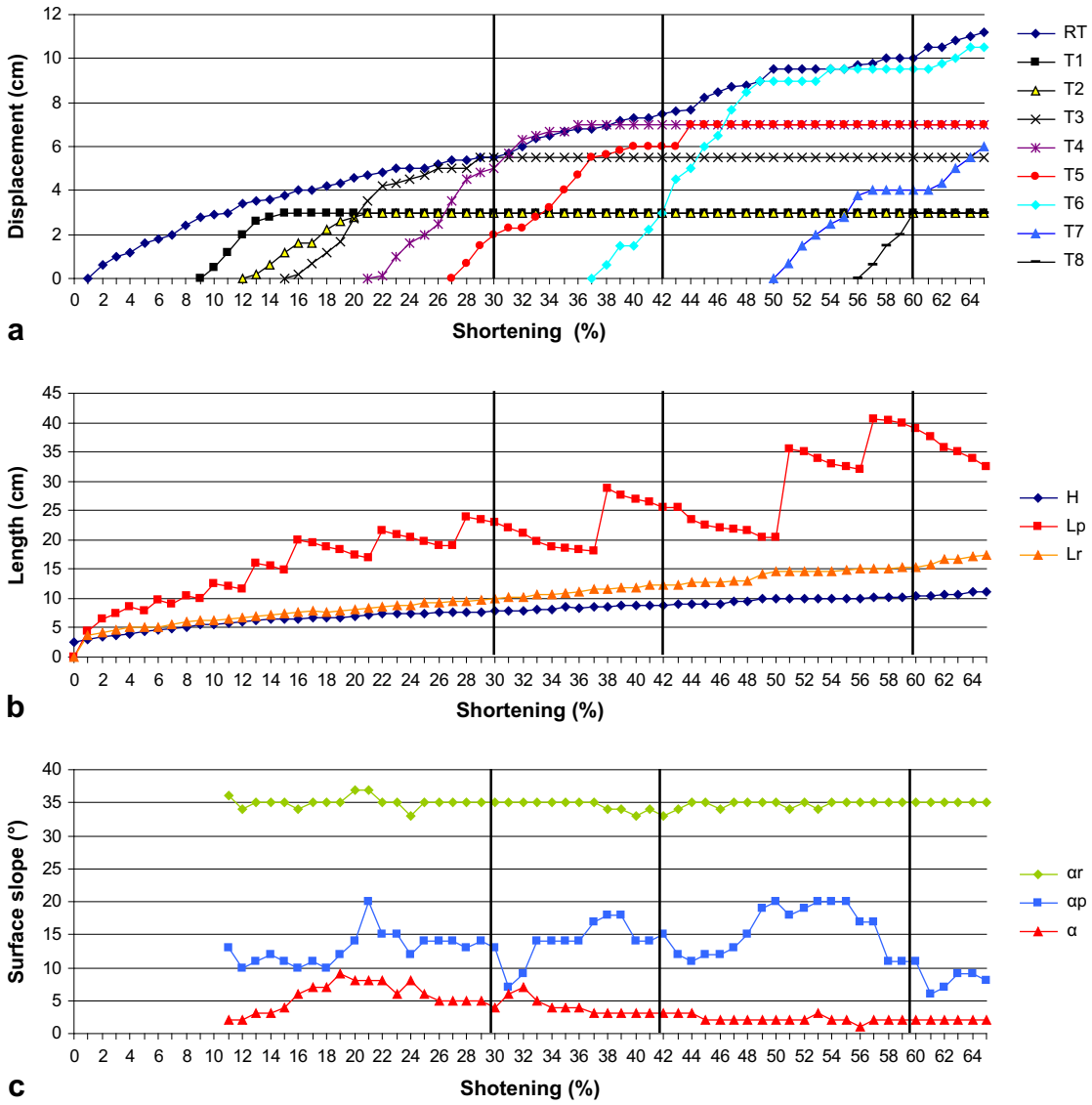

Fig. 9. Model E3. Progressive evolution of selected parameters vs. shortening: a) displacement along the retroverging ramp (RT) and along the main thrusts in the prowedge (T_n); b) height of the axial zone (H), distance of the deformation front in the prowedge (L_p) and in the retrowedge (L_r) from the subduction slot; c) surface taper of the prowedge (α_p), of the retrowedge (α_r) and of the axial zone (α). The repeated sedimentation events are marked as vertical lines. After the first one, T6 nucleation is delayed, while T4 and T5 continued their activity; similarly, after the second sedimentation event, T7 nucleation is delayed.

a severe underthrusting (along T4 and T5 and then along T6 and T7) was needed, even if this localization of shortening on the former thrusts was not enough to restore the critical height (H) in the axial zone.

At 56% of shortening the eighth thrust T8, and at 64% the ninth T9, nucleated; the experiment ended at 71% (99.4 cm) of shortening when the wedge reached its critical angle equal to 11°.

3.5. Model E5 – syntectonic erosion and sedimentation

In experiment E5, syntectonic erosion and sedimentation events were both imposed at 38% of shortening. Until that moment, wedge evolution was similar to that in previous experiments, with the formation of five main thrusts (Figs. 12 and 13). We removed the material from the axial zone and pushed the sand to fill the frontal part of the prowedge. This procedure had the aim to simulate erosion in the inner part of an orogenic wedge and sedimentation in the foreland area, maintaining the total volume of the wedge as a constant (Fig. 12). As in the previous experiment, the reduced thickness of the wedge in the axial area produced a decrease of the load on the retrowedge, whereas thickness and load increased in the prowedge area, especially on the younger structures; moreover we observed a strong increase of α, almost reaching the angle of repose of the sand (Fig. 13).

The critical taper unloaded by erosion was rebuilt during the progressive shortening by tectonic thickening (Koyi et al., 2000). This was the result partly of the reactivation, and partly of the backward rotation and uplift of the thrusts located in the eroded section of the wedge (T2, T3, T4 and T5; Fig. 13). More in detail, T2, inactive before the erosional event, was reactivated up to 43% of shortening with an incremental offset of 2.4 cm (Fig. 13). T4 and T5 are also significantly reactivated. This reactivation was needed to rebuild the height (H) of the wedge, as already observed in the E4 experiment. Moreover, from 38% to 43% of shortening, the erosional event caused a rapid retreat of the prowedge deformation front (L_p) and an increase of the value of α_p from 18° to 32°. After critical height was achieved (Fig. 13), displacement along the reactivated thrusts ceased, the wedge started to propagate again, and the value

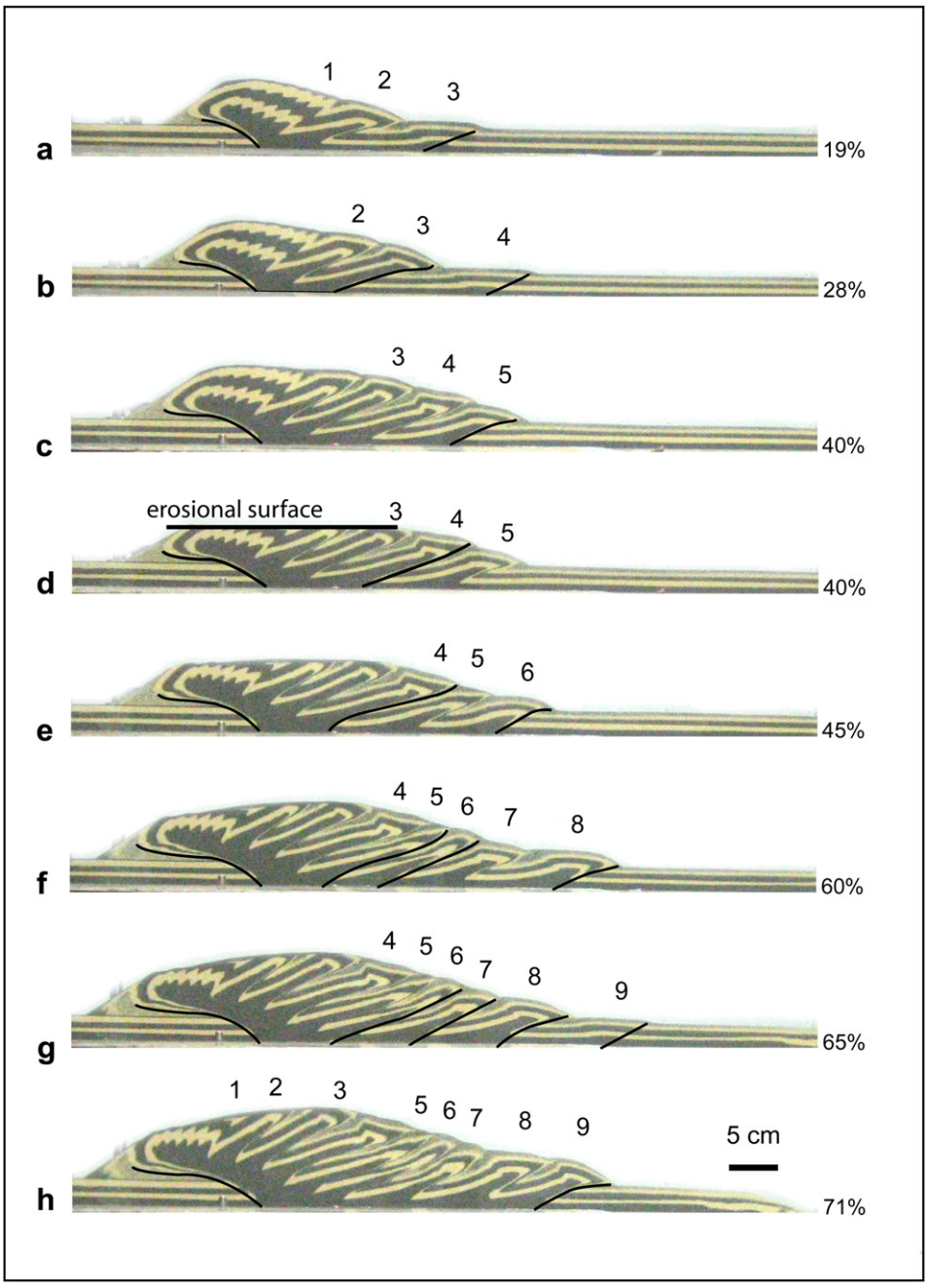

Fig. 10. Line drawing of the sequential evolution of the second stages of E4 model: a) 19% of shortening; b) 28%; c) 40%; d) 40% (immediately after the erosional episode); e) 45%; f) 60%; g) 65%; h) 71%. Thicker lines highlight active thrust at each stage of shortening.

of α started to decrease. The formation of the sixth thrust T6 occurred at 48% of shortening (after 13% of shortening), beyond the syntectonic sediments, with a long basal flat, restoring the previous asymmetry in the geometry of the wedge. The model shows a two segmented wedge involving the pre-deformation sequence; between them, the area passively filled by syntectonic sediments shows a flat geometry of the pre-deformation sequence. The seventh thrust formed at 51%, the eighth at 56%, the ninth at 61%, and the tenth at 68% of shortening (Figs. 12 and 13).

Between 65% and 70% shortening, a buried back thrust at the trailing part of T6 can be observed in Fig. 12. The geometry of this feature is very similar to the step-up of the retrothrust across the predeformation sequence and seems to be associated to a migration of the locus of maximum topography in the axial zone from prowedge toward the retrowedge in order to achieve the critical height of the axial zone.

At the end of the experiment (71%, equal to 99.4 cm) the whole wedge (pre-kinematic plus syn-kinematic sediments) showed morphology comparable with that of the others models (Fig. 14). However, considering only the pre-kinematic sand pack, wedge architecture was highly asymmetric, with a central part vertically extruded from the rest of system, and reduced ramp spacing, as in model E4 (Fig. 14).

4. Discussion

We modeled our experiments using a high basal friction value ($\mu_b = 0.55$), equal to the frictional coefficient of the modeling

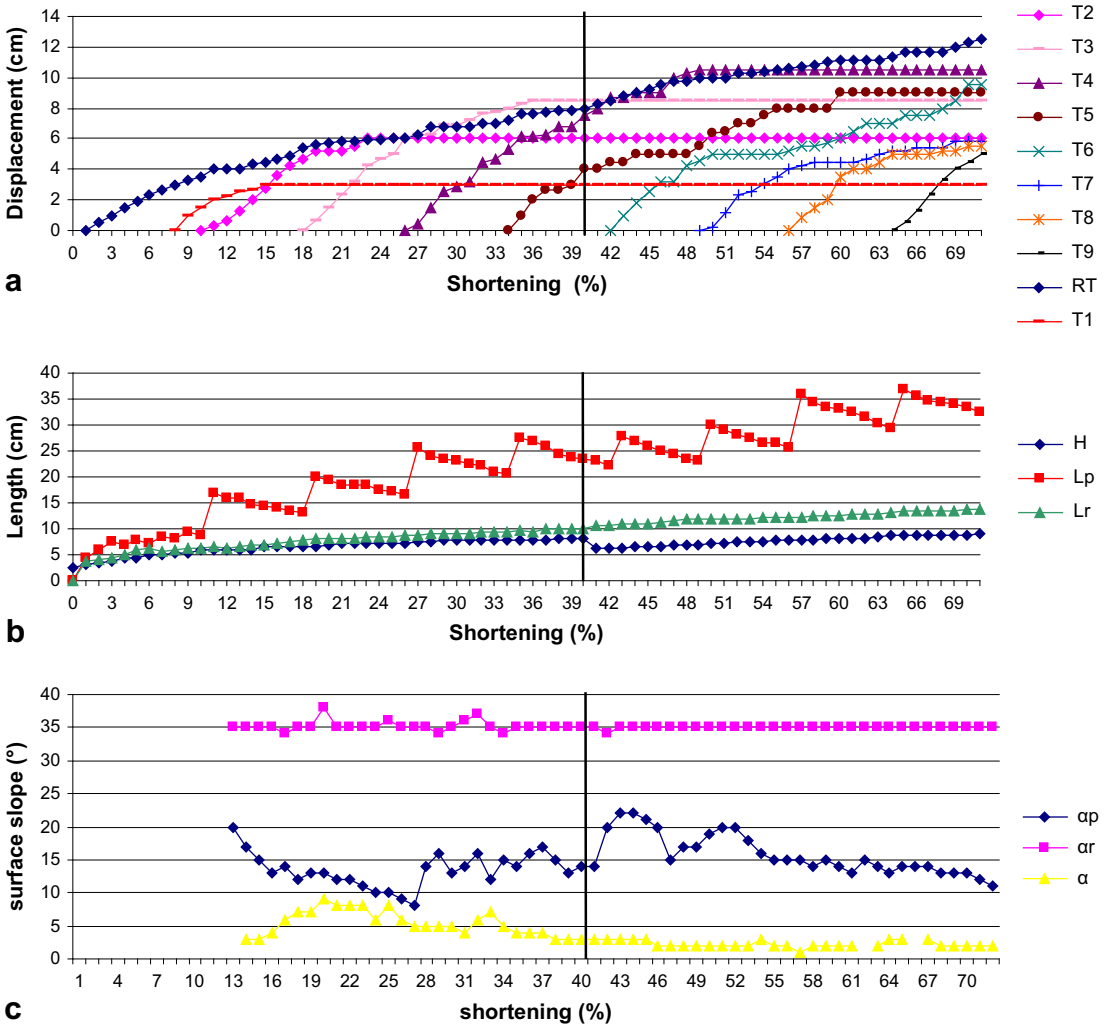

Fig. 11. Model E4. Progressive evolution of selected parameters vs. shortening: a) displacement along the retroverging ramp (RT) and along the main thrusts in the prowedge (T_n); b) height of the axial zone (H), distance of the deformation front in the prowedge (L_p) and in the retrowedge (L_r) from the subduction slot; c) surface taper of the prowedge (α_p) and of the retrowedge (α_r). The erosional episode (vertical line) pushed the growing wedge in a supercritical condition as indicated by α(p) variation triggering accretion at the toe of the prowedge and, at the same time, reducing the height of the axial zone, triggering underthrusting, as indicated by the activity of T4 and T5 thrusts.

material; as a consequence, we observed a very marked cyclical behavior especially during the second stage (prowedge accretion) in terms of variation of the length of the prowedge (position of deformation front with respect to the subduction slot, L_p) (Gutscher et al., 1996; McClay, 1990; Koyi et al., 2000). Continuous cyclicity has been interpreted either as depending upon evolving surface slope of the wedge (Gutscher et al., 1998) or as being controlled by different basal coefficient of friction (Burbidge and Braun, 2002). However, cyclicity has been observed even in experiments with a slightly lower basal coefficient of friction (Del Castello et al., 2004).

The high length/thickness ratio (140 cm/2.5 cm) allowed us to observe the whole cycle of response of the wedge to the imposed modifications of the α value and to the forced redistribution of the load along the system, especially in experiment E3, where these modifications were imposed three times during deformation. It also allowed us to impose these modifications on the system after the first phase of development, when the prowedge had already started to develop, making it possible to observe possible reactivations in the retrowedge.

All the experiments reached their critical status before 100% of shortening, which made it possible to compare final values and final geometry among the various models (Fig. 14).

4.1. Retrowedge activity

In all experiments, we observed a two-stage kinematic evolution, caused by a change in the dynamics of the system and consistent with the kinematics already described by Storti et al. (2000). At the beginning of the convergence, the experimental configuration is a homogenously horizontal multilayered sand pack. Therefore the system tends to quickly reach wedge-shape morphology through a retroverging thrust ramp accompanied by the development of closely spaced prowedge fault-related anticlines, which generate the off-hand uplift of this sector close to the backstop. Retrowedge verging translation of the prowedge and of the axial zone along the main retrowedge thrust progressively increases the load on this fault surface, thereby increasing its strength. In all the experiments, after about 10% of shortening, in the axial zone, the height H reached a critical value and the load on the retrowedge basal thrust became too great to allow further fast slip. That part of the wedge behaved as a dynamic backstop, the mechanical balance of the system changed and the deformation switched to the foreland at the front of the prowedge toe (Storti et al., 2000). The same process, although at smaller scale, can be observed in the final part of experiment E5, suggesting

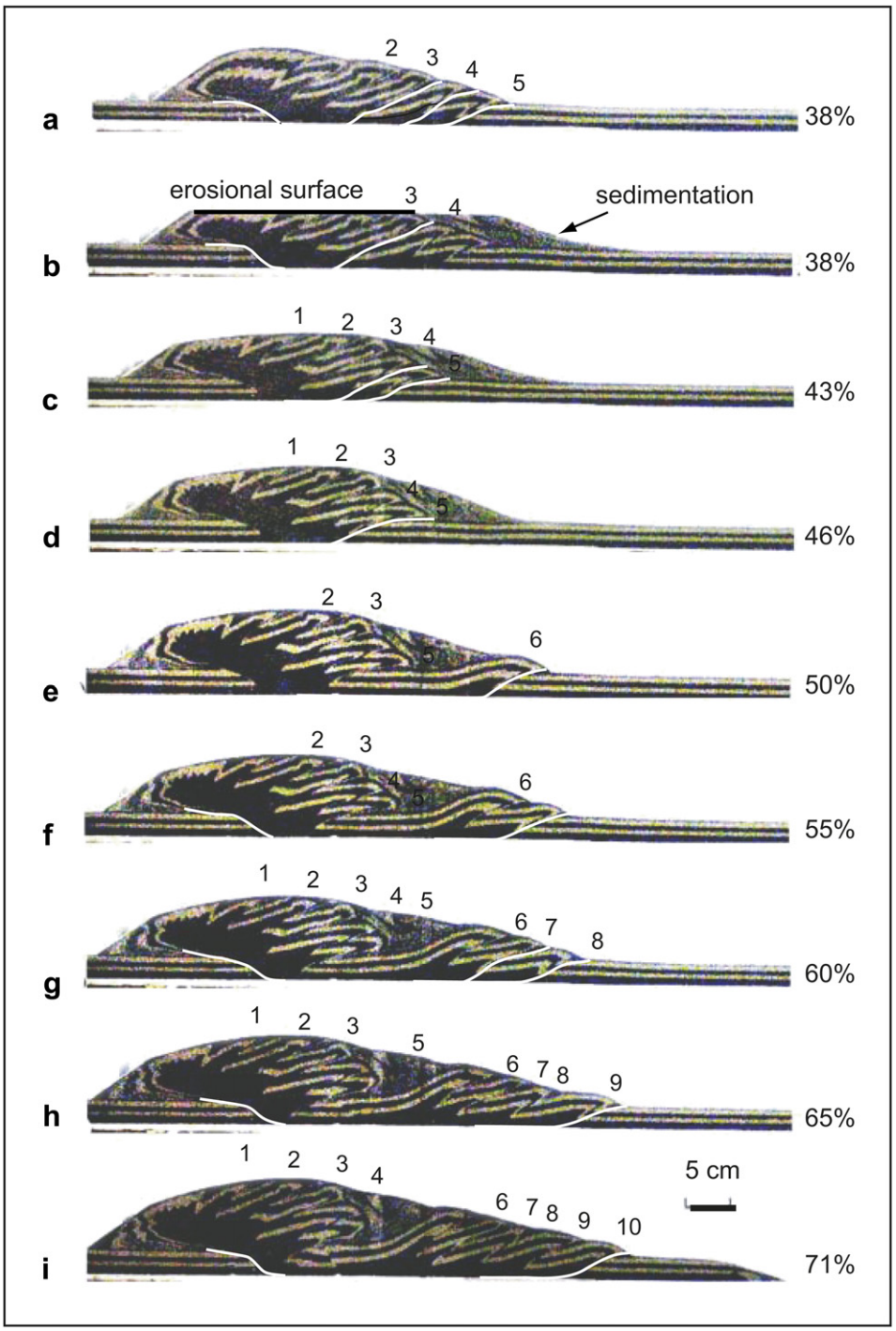

Fig. 12. Line drawing of the sequential evolution of the second stages of E4 model: a) 38% of shortening; b) 38% (immediately after the sedimentation/erosion episode); c) 43%; d) 46%; e) 50%; f) 55%; g) 60%; h) 65%; i) 71%. Thicker lines highlight active thrust at each stage of shortening. The material eroded from the top of the wedge ad deposited at the toe is in gray.

a relationship between the generation of back thrust and the impulse of reaching the critical height of equilibrium.

After the first stage, retrothrust activity of about 2 cm/4% of shortening does not stop, but continues at a slower rate of deformation during the development of the prowedge, as shown by the lower dip of the curve displacement vs. shortening in experiment E1 (less than 1 cm/4% of shortening) (Fig. 4). In E2 and in E3, instead, after each episode of sedimentation, we observed an increment of this velocity. In E2, after sedimentation at 40% of shortening, the retrothrust displacement accelerated with a rate of 2 cm/6% of shortening, comparable to the one observed during the first stage, as shown by the dip of the curve displacement vs. shortening of Fig. 6. It decelerated again when the new and more external thrust T7 started to propagate in the prowedge (Fig. 6). This behavior repeated itself in E3, after each episode of sedimentation (Fig. 9). In Fig. 9, the curve displacement vs. shortening for the retrowedge in E3, evidences steep path intervals after sedimentation; the curve flattens again when the prowedge starts to accrete. After the first episode, it steepens before the propagation of T6. After the second episode, it flattens when T7 starts to develop, whereas after the third one, the angle of the curve significantly diminishes as the retrothrust slows down again at the end of the experiment, at 65% of total shortening

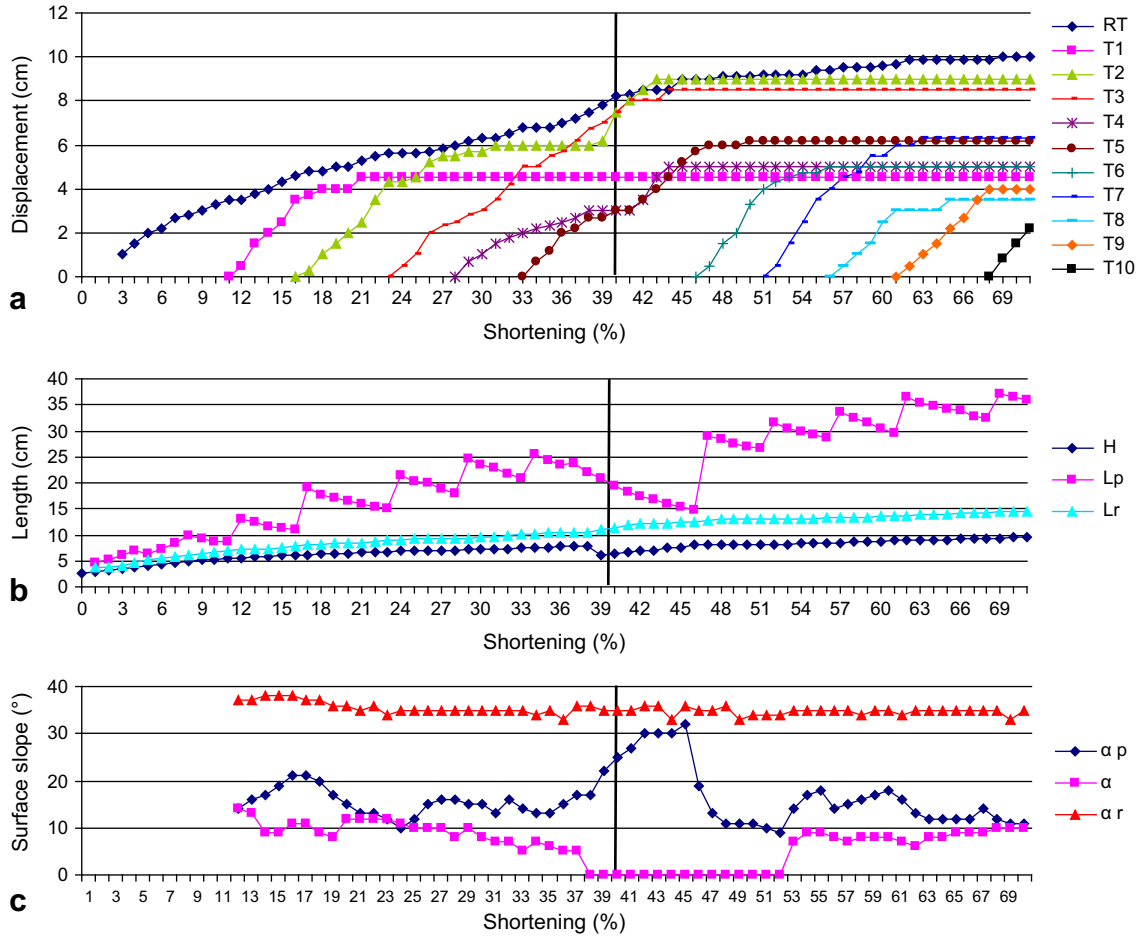

Fig. 13. Model E5. Progressive evolution of selected parameters vs. shortening: a) displacement along the retroverging ramp (RT) and along the main thrusts in the prowedge (T_n); b) height of the axial zone (H), distance of the deformation front in the prowedge (L_p) and in the retrowedge (L_r) from the subduction slot; c) surface taper of the prowedge (α_p), of the retrowedge (α_r) and of the axial zone (α). After the sedimentation/erosion episode indicated as a vertical line, redistribution of loading delayed nucleation of T6 thrust, triggered activity on all the previous thrust (from T2 to T5) and stopped the accretion in the prowedge, as indicated by L_p variation. In this way, it pushed the wedge in a supercritical condition which triggered again accretion at the toe of the prowedge, after 45% of shortening.

(Fig. 9). These observations suggest that retrothrust activity accelerated during episodes of underthrusting or reactivation of older thrusts, immediately after the episodes of sedimentation. This could be due to the load imposed on the basal detachment causing an increase of its strength under the prowedge, whereas the retrowedge areas is unloaded, with subsequent strength decrease. The impulse to reach again the critical slope value and the critical height promotes underthrusting in the prowedge and also triggers a faster activity in the retrowedge area, where the basal thrust supplies with higher increments of displacement to the total shortening. Acceleration of retrowedge is not so dramatic in E4, but there is an apparent increase in the displacement vs. shortening rate, which seems to last more than in E2 and E3. On the other side, the acceleration of the retrowedge in E5 is quite evident, and does not stop with the reactivation of previous structures, but slightly later. In these cases in fact, no extra load has been imposed on the basal detachment in the prowedge region, and the system tends to achieve a balance locally, in the same areas interested by erosion and by erosion/sedimentation episodes.

4.2. Cyclical behavior of wedge accretion

In our experiments we imposed episodes of sedimentation and/or erosion exclusively during the second evolutionary stage and on the prowedge area, in order to modify the behavior of wedge accretion, which commonly occurs in this kind of experiment (Mulugeta and Koyi, 1992; Gutscher et al., 1996, 1998; Del Castello et al., 2004; Adam et al., 2005; Naylor et al., 2005; Del Castello and Cooke, 2007). In our base model E1, during the second stage, the spaced nucleation of new anticlines at the front of the prowedge occurred in a rather regular mode, clearly visible in the saw-tooth shape of the length of the prowedge graphed in Fig. 4. A regular mode of accretion is also suggested by the ramp spacing of experiment E1, where the distance between ramps is rather constant (about 10 cm), suggesting a repeated and invariable configuration of the strengths on the basal detachment (Fig. 14). According to Mulugeta and Koyi (1992), the prowedge surface slope α shows a non steady state evolution in contrast with the critical taper theory of Davis et al. (1983). During the second stage of our experiments, incorporation of thrust sheets into the prowedge produced an episodical widening of the prowedge, whose dip (α) progressively decreased at each cycle until the critical value was reached.

Accretion of natural orogenic wedges generally occurs according to one of three end-member modes: piggy-back thrusting (Boyer and Elliott, 1982), break-back thrusting (Butler, 1987), and synchronous thrusting (Boyer, 1992). A thorough analysis of displacement curves for base model E1 shows that, despite a general piggy-back mode of accretion, some inner thrusts in the

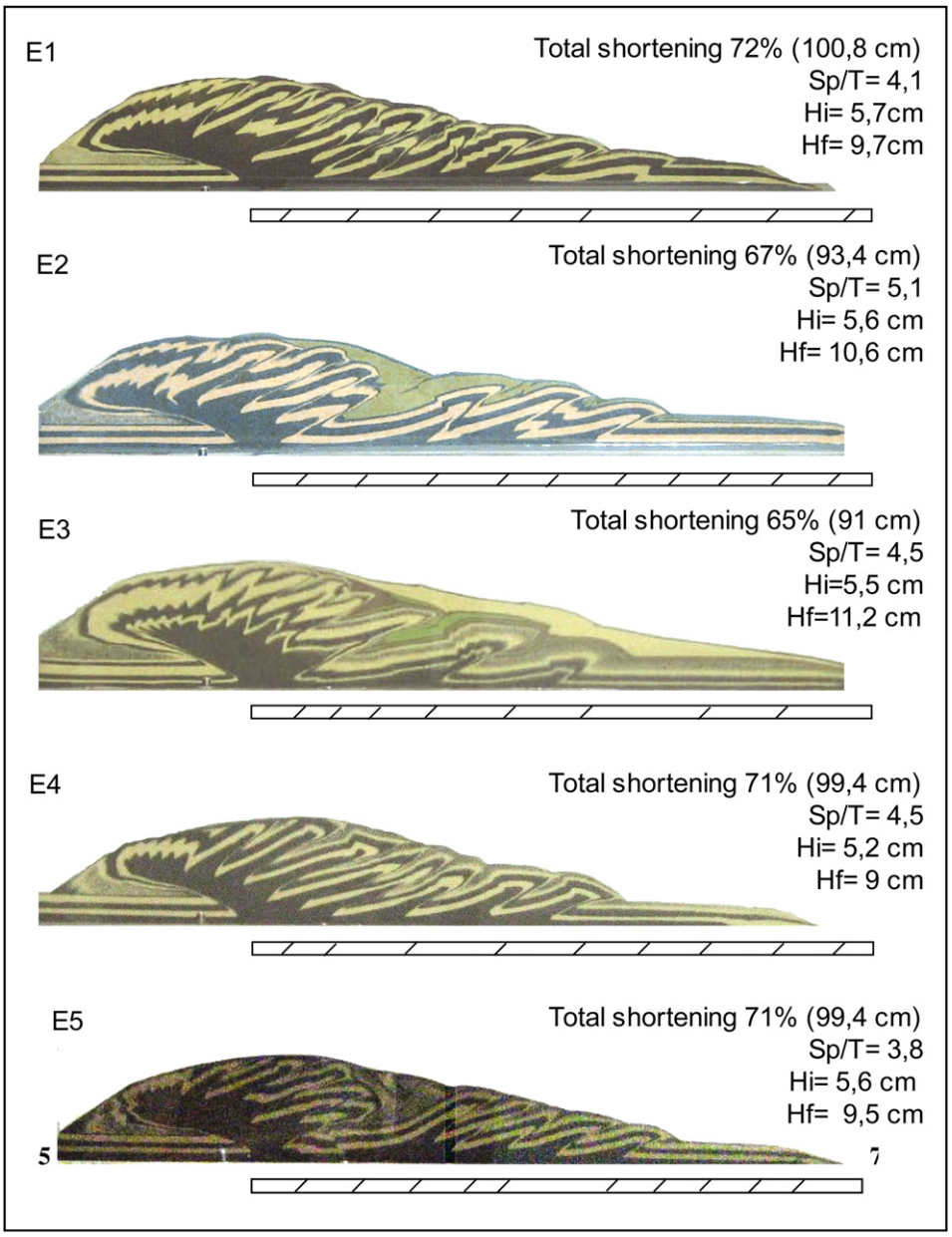

Fig. 14. Comparison of the final geometries and parameters of all the models with the sketch of ramp spacing during the second evolutionary stage (under each model). Note as the main episodes of underthrusting generated by sedimentation and/or erosion events are strongly recorded in the final geometry of the pre-deformation sequence, while the final profiles of the wedges are quite similar. Hi = height of the axial zone at the end of the first stage of evolution; Hf = height of the axial zone at the end of the second stage. Note as, although the occurrence of a strong underthrusting episode after erosion, E4 shows the lowest value, whereas the Hf of E5 is comparable to the base model E1.

prowedge remained active during accretion, and so did the basal thrust in the retrowedge, whereas other inner thrusts alternated periods of activity to periods of quiescence (i.e. T5 in model E1, Fig. 4). This periodic reactivation of inner thrusts, generally defined also as underthrusting, can be well explained as induced by the drop or rise of slope value α_p with respect to the minimum critical taper (Davis et al., 1983; Storti and McClay, 1995), and has been described through numerical models as a result of the balance of work against gravity, work of fault propagation, frictional strength acting on thrust planes, and frictional strength acting on basal detachment in order to satisfy a total work minimization of the fault system (Hardy et al., 1998; Del Castello and Cooke, 2007). Underthrusting occurred also in our base model, though characterized by a very simple configuration, suggesting it is indeed an ordinary rule of accretion, rather than the result of a modification of the system (Hardy et al., 1998). Nevertheless, in our experiments, underthrusting and break-back sequences occurred especially after modification of the systems, both by sedimentation and erosion, accompanied by an acceleration of retrothrust activity. Total load redistribution, due to sedimentation and erosion, and the interplay between the fixed basal coefficient of friction and the continuous variation of the α_p value, controlled the strength of basal detachment. Therefore it was locally and episodically deactivated, as evidenced by the increase in ramp spacing after the sedimentation episodes underneath the thicker areas as a consequence of the additional load (Fig. 14).

The addition of syntectonic sediments (E2 and E3) in front and on top of the growing imbricate wedge lowered the α_p value and increased load on the basal detachment surface. To recover the critical α_p value in model E2, the wedge grew upward by

concentrating deformation toward the rear of the wedge. The number of thrusts and the amount of total shortening in the wedge decreased with respect to E1 (Figs. 5, 6 and 14). We expected this mechanism to be observed also in model E3, where material was added three times (Figs. 8 and 9). In fact, a more complex cyclical behavior occurred, controlled by both mass balance and variation of strength resistance on the basal detachment of the prowedge. The total volume of the material added to the system in E3 is close to that added in one event in model E2; in both E2 and E3 the same number of thrusts had developed at the end of the model run (Fig. 14). The total shortening was similar too, suggesting a direct correspondence between the total mass of the system and the total displacement expressed by the wedge (Del Castello et al., 2004). The same was true for the critical slope α_p value measured at the end of the model runs, with a difference of one degree between E2 (9°) and E3 (8°) (Fig. 14).

In model E3, the cyclical behavior of the wedge observed in E2 after the sedimentation episode, repeated itself each time with different amplitude, depending on the location of the sedimentary load and the volume of the material added at each event (Figs. 8 and 9). In the first and second sedimentation episode, maximum thickness of the added sediments corresponded to the toe of the already formed wedge ahead of thrust T5, in the first episode and of thrust T6 in the second one (Fig. 8) and the response is a persistent activity on the same thrusts, until the formation of a new thrust ahead of the previous ones. In experiment E3, after the third episode of sedimentation, the thickness of the added sediments was more uniform over the wedge; this caused the final lock of the last T8 and localized underthrusting along T7 and T3 (Figs. 8 and 9).

In model E4, erosion in the axial area reduced the total mass of the system and the height of the wedge, causing the reactivation of the inner thrusts until the re-establishing of critical values in the inner zone (surface slope and height of the axial zone) (Figs. 10 and 11). In this case, however, underthrusting did not deactivate frontal accretion: all thrusts activated and reactivated after the erosion episode remained active until the end of the model run (Fig. 11). We interpret this as due to the volume of removed material which was not enough to lock movement along the prowedge basal detachment, but enough to redistribute a rather homogeneous load along the wedge. In the same way, even when the wedge volume was kept smaller, a longer coeval activity of outermost thrusts and a clear underthrusting of entire thrust units was observed (Fig. 11). Unexpectedly, this allowed the wedge to maintain a regular cyclicity of its length variation as shown in Fig. 10, despite the value of final height in the axial zone, which was less than in E1. Coeval underthrusting and frontal accretion is the fastest way for the system to recover from the loss of its relative equilibrium imposed by the sudden erosion of the axial zone. Underthrusting is enhancing the recovery of the critical height, and frontal thrusts are required to reach the prowedge critical angle. Furthermore, vertical load in the prowedge area is not changed with respect to model E1, and thus the basal strength might remain unmodified, as suggested by the regular spacing of the thrust sheets, almost identical to E1 (Figs. 11 and 14).

The coeval erosion and re-deposition we performed in model E5 changed the pattern of strain partitioning in the wedge and therefore affected thrust geometry and distribution of shortening, but kept constant the total mass of the system. Local re-deposition of the same eroded material increased the vertical load at the toe of the wedge and, at the same time, decreased load and height (H) in the axial zone. In this case, this new mass distribution provoked a lock of the basal detachment and, in the prowedge, a long phase of underthrusting (re-activation of previous thrusts), retarding the accretion of a new thrust fault at the toe of the wedge (Figs. 12–14). After this episode, the wedge behavior was very similar to that observed in experiments E2 and E3, with marked activation of underthrusting and substantial deactivation of frontal accretion. Having reached critical values again, the wedge started once more to propagate in a regular fashion (Fig. 14). The surface slope and the amount of shortening are quite similar to base model E1, suggesting that the wedge had enough time to reorganize its external geometry as a function of the total mass of the system and its internal parameters (internal and basal detachment strength) in agreement with the Coulomb wedge theory (Fig. 14).

4.3. Implications for natural orogens

Sedimentation and erosion episodes recorded in sedimentary successions are the tool usually adopted to reconstruct the evolution and kinematics of fold-and-thrust belts (i.e. Patacca and Scandone, 2001 and references therein). In the Apennines for example, the progressive time-space migration of the orogenic system is recorded by foredeep deposits. At the same time, the occurrence of thick sedimentary successions accumulated on and at the front of the growing wedge can be the control factor of the tectonic activity distribution of the thrusts of the chain. In this way is possible to interpret the tectonic cycle described by Patacca and Scandone (2001) for the Southern Apennines, where the mechanisms of deactivation of the frontal ramp and the underthrusting is largely documented. A similar sequence of thrusting is described by Tesòn and Teixell (2008) for the SubAtlas thrust belt in Marocco, where the exposed faults show evidence of a complex, synchronous sequence with events of fault reactivation and out-of-sequence thrusting controlled by sedimentation and erosional processes. Similar results are described by Bonnet et al. (2007) where the study of the interaction among tectonics, sedimentation and erosion was used to describe the evolution of the Alpine orogen.

5. Conclusion

Scaled analogue models have been employed to investigate cyclicity and its modification in the evolution of a growing sand wedge after episodes of sedimentation and/or erosion. The adoption of a high length/thickness ratio (140 cm/2.5 cm) of the sand pack allowed us to observe the whole cycle of response of the wedge to the imposed modification of the α_p value and to the forced redistribution of the load along the system. All modifications were imposed during the second stage of evolution. During this stage a regular cyclicity in the prowedge accretion was observed, including in model E1.

In Fig. 13, experimental results are synthesized comparing the general configurations of the models. The results show that cyclicity is determined by wedge parameters directly influenced by internal and basal coefficients of friction, whereas the mode of accretion, which tends to be cyclical too, can be considered as the main factor for the re-achievement of the equilibrium after the modification of the system.

Syn-contractional sediments lowered the number of thrusts (from 10 in E1 to 8 in E2 and E3), the amount of final shortening (72% in the E1, 67% in the E2 and 65% in the E3) and the critical topographic slope (10° in the E1, 9° in the E2 and 8° in the E3), which indicates that these features modified the initial boundary conditions, as predicted by the Coulomb wedge theory (total volume, internal and basal friction). Moreover, sedimentation episodes imposed in E2 and E3 show how distribution of vertical load basically controls the accretion mode, which switches from frontal accretion to synchronous thrusting and underthrusting immediately after sedimentation episodes (Storti et al., 2000; Del Castello et al., 2004). The shortening span of the recovery cycle, marked by strong underthrusting coeval to the stop of frontal accretion, is clearly related to the volume of the added material and

of its location on the growing wedge, and a recovery cycle with similar characteristics was observed also in the E5 experiment. More specifically, in the E5 experiments case, after coeval sedimentation in foredeep zone and erosion in the axial zone, we observed a marked switch from frontal accretion to underthrusting, leading the wedge to a supercritical condition, and then to again to frontal accretion again, as required by the system to progressively reduce the surface slope value.

In experiment E4, the erosional episode redistributed vertical load across the whole growing wedge, triggering at the same time frontal accretion and underthrusting (Figs. 10 and 11). From that moment until the end of the experiment, wedge activity was characterized by coeval modes of accretion, even if the frontal accretion component maintained its cyclicity unaltered (Fig. 11). This allowed model E4 to reach a total shortening value comparable to that of base model E1, while exhibiting a lower height in the axial zone (Fig. 14).

Acknowledgements

This work was performed at Analogue Laboratory of the University of Roma Tre, Italy. We are grateful to Claudio Faccenna, Francesca Funiciello, Fabrizio Storti and Valerio Acocella for their hearty welcome to the lab, for their numerous suggestions and their patience. Criticism by Mario Del Castello, Eugenio Carminati and Claudio Chiarabba of an early draft of this paper, and discussion with all the above persons were much appreciated. We thanks Gabriele Poole for the final revision of English. We also wish to thank Peter Cobbold and the anonymous reviewer for their thoughtful reviews.

References

Adam, J.J.L., Urai, B., Wieneke, O., Oncken, K., Pfeiffer, N., Kukowski, J., Lohrmann, S., Hoth, W., van der Zee, J., Schmatz, J., 2005. Shear localization and strain distribution during tectonic faulting-new insights from granular-flow experiments and high resolution optical image correlation techniques. Journal of Structural Geology 27, 283–301.

Beaumont, C., Kooi, H., Willet, S., 1999. Progress in coupled tectonic-surface process models with application on rifted margins and collisional orogens. In: Summerfield, M.A. (Ed.), Geomorphology and Global Tectonics. John Wiley, New York.

Bigi, S., Lenci, F., Doglioni, C., Moore, J.C., Carminati, E., Scrocca, D., 2003. Decollement depth vs. accretionary prism dimension in the Apennines and the Barbados. Tectonics 22 (2), 1010. doi:10.1029/2002TC001410.

Bonnet, C., Malavieille, J., Mosar, J., 2007. Interactions between tectonics, erosion, and sedimentation during the recent evolution of the Alpine orogen: analogue modelling insights. Tectonics 26, TC6016. doi:10.1029/2006TC002048.

Boyer, S.E., Elliott, D., 1982. Thrust systems. American Association of Petroleum Geologists Bulletin 66, 1196–1230.

Boyer, S.E., 1992. Geometric evidence for synchronous thrusting in the southern Alberta and northwest Montana thrust belts. In: McClay, K. (Ed.), Thrust Tectonics. Chapman and Hall, New York.

Burbidge, D.R., Braun, J., 2002. Numerical models of the evolution of accretionary wedges and fold-and-thrust belts using the distinct-element method. Geophysical Journal International 148, 542–561.

Butler, R.W.H., 1987. Thrust sequences. Journal of Geological Society of London 144, 619–634.

Calassou, S., Laroque, C., Malavieille, J., 1993. Transfer zones of deformation in thrust wedges: an experimental study. Tectonophysics 221, 325–344.

Chapple, W.M., 1978. Mechanics of thin-skinned fold-and-thrust belts. Geological Society of American Bulletin 89, 1189–1198.

Dahlen, F.A., 1984. Non cohesive critical Coulomb wedges: an exact solution. Journal of Geophysical Research 89, 10125–10133.

Dahlen, F.A., 1990. Critical taper model of fold-and-thrust belts and accretionary wedges. Annual Review of Earth and Planetary Sciences 18, 55–99.

Dahlen, F.A., Suppe, J., Davis, D., 1984. Mechanics of fold and thrust belts and accretionary wedges: cohesive Coulomb theory. Journal of Geophysical Research 89, 10087–10101.

Davis, D.M., Suppe, J., Dahlen, F.A., 1983. Mechanics of fold-and-thrust belts and accretionary wedges. Journal of Geophysical Research 88, 1153–1172.

De Celles, P.G., Giles, K.A., 1996. Foreland basin systems. Basin Research 8, 105–123.

Del Castello, M., Pini, G.A., McClay, K.R., 2004. Effect of unbalanced topography and overloading on Coulomb wedge kinematics: insights from sandbox modeling. Journal of Geophysical Research 109, B05405. doi:10.1029/2003JB002709.

Del Castello, M., Cooke, M.L., 2007. Underthrusting-accretion cycle: work budget as revealed by the boundary element method. Journal of Geophysical Research 112, B12404. doi:10.1029/2007JB004997.

Doglioni, C., Gueguen, E., Harabaglia, P., Mongelli, F., 1999. On the origin of W-directed subduction zones and applications to the western Mediterranean. Special Publication. Journal of Geological Society 156, 541–561.

Frizon De Lamotte, D., 2005. About the Cenozoic inversion of the Atlas domain in North Africa. Comptes Rendus Geosciences 337, 475–476.

Goff, D., Wiltschko, D.V., 1992. Stress beneath a ramping thrust sheet. Journal of Structural Geology 14, 437–449.

Graveleau, F., Dominguez, S., 2008. Analogue modelling of the interaction between tectonics, erosion and sedimentation in foreland thrust belts. C.R. Geoscience 340, 324–333.

Gutscher, M.A., Kukowski, N., Malavieille, J., Lallemand, S., 1996. Cyclical behavior of thrust wedges: insight from high basal friction sandbox experiments. Geology 24, 135–138.

Gutscher, M.A., Kukowski, N., Malavieille, J., Lallemand, S., 1998. Episodic embricate thrusting and underthrusting: analog experiments and mechanical analysis applied to the Alaskan accretionary wedge. Journal of Geophysical Research 103, 10161–10176.

Hardy, S., Duncan, C., Masek, J., Brown, D., 1998. Minimum work, fault activity and the growth of critical wedges in fold and thrust belt. Basin Research 10, 365–373.

Konstantinovskaia, E., Malavieille, J., 2005. Erosion and exhumation in accretionary orogens: experimental and geological approaches. Geochemistry, Geophysics and Geosystems 6, Q02006. doi:10.1029/2004GC000794.

Koyi, H., 1995. Mode of internal deformation in sand wedges. Journal of Structural Geology 17, 293–300.

Koyi, H., Hessami, K., Teixell, A., 2000. Epicenters distribution and magnitude of earthquakes in fold-thrust belts: insights from sandbox models. Geophysical Research Letters 27 (2), 273–276.

Kukowski, N., von Huene, R., Malavieille, J., Lallemand, S.E., 1994. Sediment accretion against a buttress beneath the Peruvian continental margin at 12° S as simulated with sandbox modelling. Geologische Rundschau 83, 822–831.

Lallemand, S.E., Schntirle, P., Malavieille, J., 1994. Coulomb theory applied to accretionary and non accretionary wedges: possible causes for tectonic erosion and/or frontal accretion. Journal of Geophysical Research 9, 12033–12055.

Larroque, C., Calassou, S., Malavieille, J., Chanier, F., 1995. Experimental modelling of forearc basin development during accretionary wedge growth. Basin Research 7, 255–268.

Lenci, F., Doglioni, C., 2007. On some geometric prism asymmetries. In: Lacombe, O., Lavé, J., Roure, F., Verges, J. (Eds.), Thrust Belts and Foreland Basins: From Fold Kinematics to Hydrocarbon Systems. Frontiers in Earth Sciences. Springer, pp. 41–60.

Liu, H., McClay, K.R., Powell, D., 1992. Physical models of thrust wedges. In: McClay, K.R. (Ed.), Thrust Tectonics. Chapman and Hall, New York, pp. 71–81.

Malavieille, J., 1984. Modélisation expérimentale des chevauchements imbriqués: Application aux chaînes de montagnes. Bulletin de la Société Géologique de France 7, 129–138.

Malavieille, J., Larroque, C., Calassou, S., 1993. Modélisation expérimentale des relations tectonique/sedimentation entre bassin avant-arc et prisme d'accretion. Comptes Rendus du l'Academie des Sciences Paris 316 (II), 1131–1137.

McClay, K.R., Whitehouse, P.S., 2004. Analogue modeling of doubly vergent thrust wedges. In: McClay, K.R. (Ed.), Thrust Tectonics and Hydrocarbon Systems. Memoir of American Association of Petroleum Geologists, vol. 82, pp. 184–206.

McClay, K., Dooley, T., Whitehouse, P., April 26–29, 1999. Analogue modeling of thin and thick-skinned thrust systems. Thrust Tectonics 99 Abstract, Egham, U.K.

McClay, K.R., 1990. Extensional fault systems in sedimentary basins: a review of analogue model studies. Marine and Petroleum Geology 7, 206–233.

Mugnier, J.L., Baby, P., Colletta, B., Vinour, P., Bale, P., Leturmy, P., 1997. Thrust geometry controlled by erosion and sedimentation: a view from analogue models. Geology 25, 427–430.

Mulugeta, G., 1988a. Squeeze box in a centrifuge. Tectonophysics 148, 323–335.

Mulugeta, G., 1988b. Modeling the geometry of Coulomb thrust wedges. Journal of Structural Geology 10, 847–859.

Mulugeta, G., Koyi, H., 1987. Three dimensional geometry and kinematics of experimental piggyback thrusting. Geology 15, 1052–1056.

Mulugeta, G., Koyi, H., 1992. Episodic accretion and strain partitioning in model sand wedge. Tectonophysics 202, 319–333.

Muñoz, J.A., 1992. Evolution of a continental collision belt: ECORS-Pyrenees crustal balanced cross section. In: McClay, K.R. (Ed.), Thrust Tectonics. Chapman and Hall, London, pp. 235–246.

Naylor, M., Sinclair, H.D., Willet, S., Cowie, P.A., 2005. A discrete element model for orogenesis and accretionary wedge growth. Journal of Geophysical Research 110, B12403. doi:10.1029/2003JB002940.

Patacca, E., Scandone, P., 2001. Late thrust propagation and sedimentary response in the thrust-belt-foredeep system of the Southern Apennines (Pliocene–Pleistocene). In: Vai, G.B., Marini, P. (Eds.), Anatomy of an Orogen: The Apennines and Adjacent Mediterranean Basins, vol. 401. Kluwer Academic Pub, Great Britain, p. 440.

Persson, K.S., Sokoutis, D., 2002. Analogue models of orogenic wedges controlled by erosion. Tectonophysics 356, 323–336.

Platt, J.P., 1988. The mechanics of frontal imbrication: a first-order analysis. Geologische Rundschau 77, 577–589.

Storti, F., 1997. Simulazione di anticlinali di rampa e cunei di accrezione mediante modellizzazione analogica. Bollettino Società Geologica Italiana 116, 17–38.

Storti, F., McClay, K., 1995. The influence of sedimentation on the growth of thrust wedges in analogue models. Geology 23, 999–1003.
Storti, F., McClay, K., Salvini, F., 1995. Fault-related folding in analogue models. Terra Nova 7 (1), 272.
Storti, F., Salvini, F., McClay, K., 2000. Synchronous and velocity-partitioned thrusting and thrust polarity reversal in experimentally produced, doubly-vergent thrust wedges: implications for natural orogens. Tectonics 19 (2), 378–396.
Tesòn, E., Teixell, A., 2008. Sequence of thrusting and syntectonic sedimentation in the eastern Sub Atles thrust belt (Dades and Mgoun valleys, Marocco). International Journal of Earth Science 97, 103–113. doi:10.1007/s00531-006-0151-1.
Wang, W., Davis, D., 1996. Sandbox model simulation of forearc evolution and non critical wedges. Journal of Geophysical Research 101, 11329–11339.
Westbrook, G.K., Ladd, J.W., Buhl, P., Bangs, N., Tiley, G.J., 1988. Cross-section of an accretionary wedge: Barbados Ridge complex. Geology 16, 631–635.
Willet, S., Beaumont, C., Fullsack, P., 1993. Mechanical model for the tectonics of doubly vergent compressional orogens. Geology 21, 371–374.
Willet, S.D., 1992. Dynamic and kinematic growth and change of a Coulomb wedge. In: McClay, K.R. (Ed.), Thrust Tectonics. Chapman and Hall, London, pp. 19–31.